Effect of the Inert Gas Adsorption on the Bilayer Graphene to the Localized Electron Magnetotransport

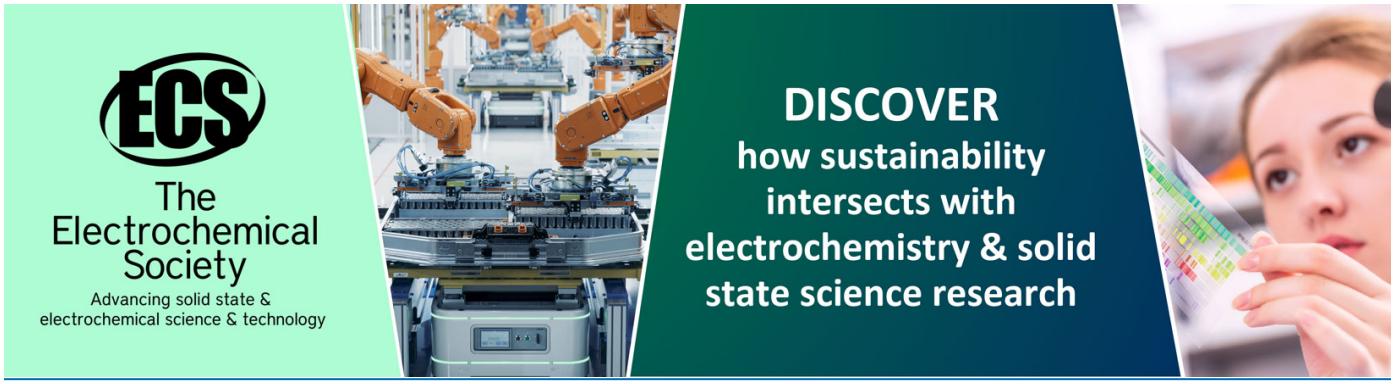

Journal of Physics: Conference Series **568** (2014) 052009 doi:10.1088/1742-6596/568/5/052009

Effect of the Inert Gas Adsorption on the Bilayer Graphene to the Localized Electron Magnetotransport

A Fukuda[1], D Terasawa[1], Y Ohno[2], K Matsumoto[2]

[1] Department of Physics, Hyogo College of Medicine, 1-1 Mukogawacho, Nishinomiya, Hyogo 663-8501, Japan

[2] The Institute of Scientific and Industrial Research, Osaka University, 8-1 Mihogaoka, Ibaraki, Osaka 567-0047, Japan

E-mail: fuku@hyo-med.ac.jp

Abstract. Graphene has a fascinating property that the two-dimensional electron gas is easily accessible externally and it is challenging to investigate the effects of the adsorption of inert gases on graphene, which may be the least effective chemically and physically. We carry out the magnetotransport measurements of ^{4}He-adsorbed bilayer graphene at low temperatures and the magnetic field B ranging from 0 to 4 T. The magnetoresistance ΔR_{xx} change from the pristine graphene is measured as a function of gate voltage $V_{\rm g}$ and B for partial coverage of 1/10 (= 0.1) layers and one layer ^{4}He-adsorbed graphene. The overall magnitudes of ΔR_{xx} for one layer are larger than the one for 1/10 layers. Signs of ΔR_{xx} depend on the $V_{\rm g}$ for the entire range of B, associated with the magnetoresistance oscillation owing to the weak localization in the pristine graphene.

1. Introduction

The experimental and theoretical studies of graphene, a two-dimensional (2D) monolayer of carbon atoms tightly packed into a honeycomb lattice, have attracted a major interest of modern condensed-matter physics, since an unusual quantum Hall effect (QHE) in high magnetic field was discovered in 2005 by two different groups[1, 2]. The most salient features of graphene contains the pseudo-relativistic physics performed by the massless Dirac fermions. The pseudo-relativistic QHE is understood in terms of Landau quantization for massless Dirac fermions, which is on the theoretical basis on the electron-electron interactions. In the case of bilayer graphene, unconventional QHE was found with massive chiral fermions with Berry's phase 2π[3]. On the contrary, in low magnetic field, weak localization (WL) dominates the transport properties of graphene. The interference of electron waves that are scattered by disorders or impurities, and form closed trajectories, usually decreases the conductivity, resulting in the WL of electrons. A negative magnetoresistance as a signature of WL was reported including the electroneutrality region in the bilayer graphene[4]. The WL in the bilayer graphene was also theoretically investigated[5].

Another remarkable feature of graphene is the accessibility to the two-dimensional electron gas (2DEG) from outside. Though the 2DEG in the conventional semiconductor heterostructures such as GaAs/AlGaAs is known to have an extremely high mobility, it has been rather difficult

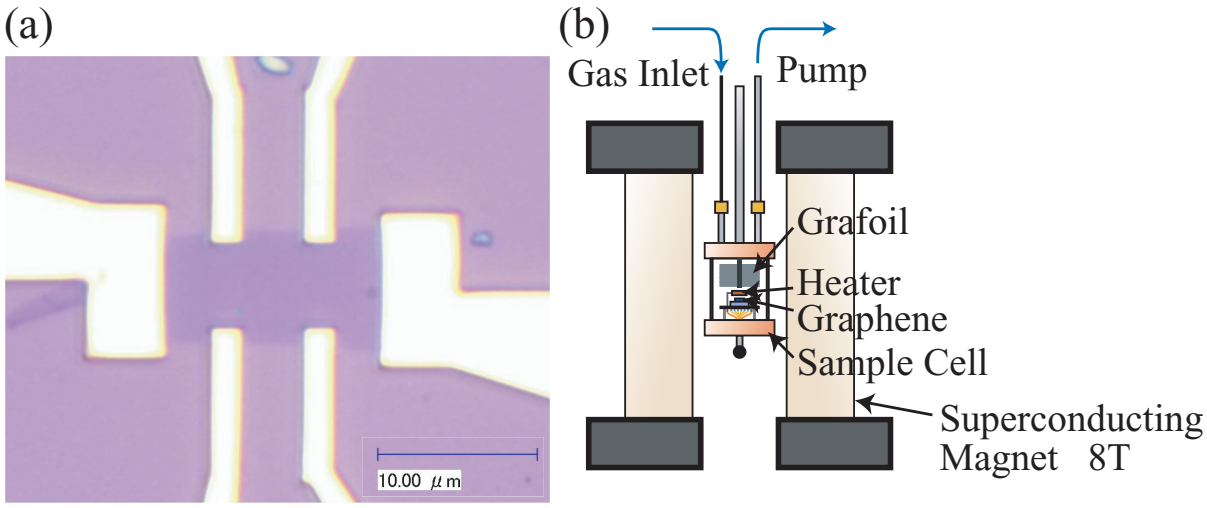

Figure 1. (a) Optical microscope image of our exfoliated graphene device. (b) Design of the cryostat for transport measurements of graphene device with ^{4}He atom adsorption.

to access directly from the outside probe such as a scanning tunnel microscope. Graphene is a promising material not only to solve this problem but also to study the effects of the adsorption or chemical adjunction of various kinds of molecules on graphene. Therefore, to study the transport properties with an adsorption or chemical modification by external molecules on graphene is intriguing. Shedin *et al.* demonstrated that micrometre-size sensors made from graphene are capable of detecting individual events when a gas molecule such as CO, NH_3, H_2O, NO_2 attaches to or detaches from graphene's surface[6]. Another prominent achievement is findings of the evidence of hydrogenated graphene called "graphane"[7], where the appearance and the disappearance of the QHE are fully controllable by reversible hydrogenation. Applied techniques are utilized for such as an electrical detecting pH and protein adsorptions[8] or a selective permeation of water[9]. These works envision us the higher feasibility of graphene-based gas sensors with an ultimate sensitivity. Therefore, it is most challenging but has been less explored to investigate the effects of the adsorption of an inert gas on graphene, which may be the least effective to the transport properties.

In this report, we observe the magnetotransport of ^{4}He-adsorbed bilayer graphene at low temperatures and under the magnetic field B ranging from 0 to 4 T. We measure the ΔR_{xx}, the difference of the magnetoresistance R_{xx} between the pristine graphene and helium adsorbed graphene, where the layer number of adsorbed atoms is precisely controlled. We discuss the relationship between ΔR_{xx} and the weak localization effect of 2DEG transport. We also remark the possibility to utilize the graphene device as a highly sensitive sensor for adsorbed gas as a powerful tool of the condensed matter physics.

2. Experiments

The bilayer graphene is fabricated by the mechanical exfoliation method[10] onto the surface of SiO_2 300 nm apart from the n^+ doped Si substrate. Optical microscope image of our exfoliated graphene device is shown in Fig. 1(a). We choose a natural bilayer graphene flake that has almost a rectangular shape. We fabricate a Hall bar with the dimension of 13 μm-long for the source - drain electrodes, 5 μm-long for the longitudinal voltage electrodes, and 7 μm-wide for the Hall voltage electrodes. The contact pattern is depicted by electron beam lithography. The ohmic contact materials (10 nm of Ti followed by 100 nm of Au) are deposited by thermal evaporation then followed by liftoff in warm 1-methyl-2-pyrrolidone. The number of the layers

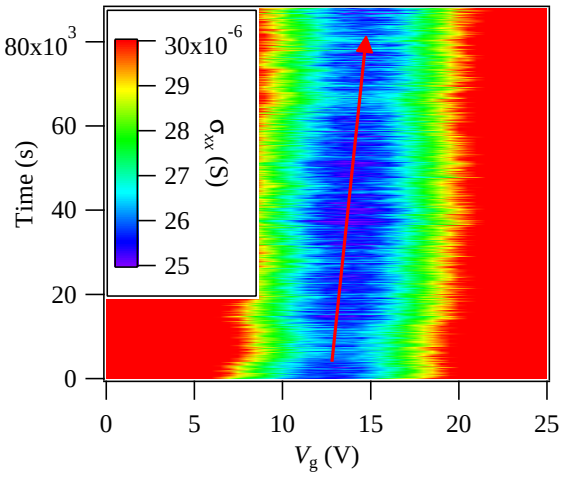

Figure 2. Displacement of the charge neutral point (CNP). Time evolution of the conductivity σ_{xx} as a function of gate voltage $V_{\rm g}$ is demonstrated.

is confirmed by the Raman shift spectra[11]. The sample is first annealed at 700 K in the H_2 atmosphere for 30 minutes.

Overview of our cryostat for the transport measurements of graphene with gas adsorption is illustrated in Fig. 1(b). The sample is placed in the vacuum-tight sample cell with an external heater and a grafoil sheet having large effective areas of 1.2 m^2. The grafoil sheet is utilized to regulate and determine the precise number of layers of adsorbed molecules. The heater inside the sample cell enables us *in situ* annealing even at low temperatures. The sample is annealed again by using this heater for two hours at 410 K before it is cooled down. Resistances are measured by a standard ac lock-in technique of 4-terminal measurements with a frequency of 37 Hz. Carrier densities are controlled by the back gate voltage $V_{\rm g}$ applied between the graphene sheet and the substrate. The helium-free Gifford-MacMahone (GM) refrigerator is used to cool down the sample as well as the superconductor magnet with the maximum magnetic field of 8 T. The magnetic field is applied up to 4 T in this experiment.

Using the relationship between the carrier density n and the gate voltage $n = (C/e) \cdot V_{\rm g} = 7.2 \times 10^{10}\, V_{\rm g}\, {\rm cm}^{-2}$, where C denotes the capacitance of 300-nm thick SiO_2 and e denotes the elementary charge, the carrier density at 18V apart from the charge neutral point (CNP) is estimated to be $1.3 \times 10^{16}\, {\rm cm}^{-2}$. Thus the mobility of the sample at room temperature is estimated to be $2500\, {\rm cm}^2/{\rm Vs}$.

3. Results and Discussions

First, to check the sensitivity of our graphene device for an adsorption of the external gas molecules at room temperature, we investigate the conductivity σ_{xx} change induced by the air adsorption at the field B of 0 T, followed by the well-annealed process mentioned above, while we monitor that the CNP moves to the lower voltage. Figure 2 demonstrates the time t evolution of σ_{xx} for gate voltage $V_{\rm g}$ sweep, where the graphene is exposed to air at the constant pressure $P = 815$ Pa. At $t = 0$ sec, the minimum of σ_{xx} is located at $V_{\rm g} = 12.5\,{\rm V}$, which is located at the CNP. At $t = 8.78 \times 10^4$ sec, the CNP moves to $V_{\rm g} = 14.5\,{\rm V}$, indicated by a red arrow in Fig. 2. Therefore, the velocity of the CNP displacement $dV_{\rm g}^{\rm CNP}/dt = 2.3 \times 10^{-5}{\rm V/s}$. Subsequent experiments reveal that the quantity of $dV_{\rm g}^{\rm CNP}/dt$ sensitively depends on the gas pressure P, where $dV_{\rm g}^{\rm CNP}/dt$ increases as P increases.

Next, we cool down the device of a graphene to about 7 K and observe the temperature dependence of the resistance R_{xx}. Figure 3 presents the R_{xx} as a function of $V_{\rm g}$ for various temperature T. The position of the CNP $V_{\rm g}^{\rm CNP}$ is almost temperature independent. Above

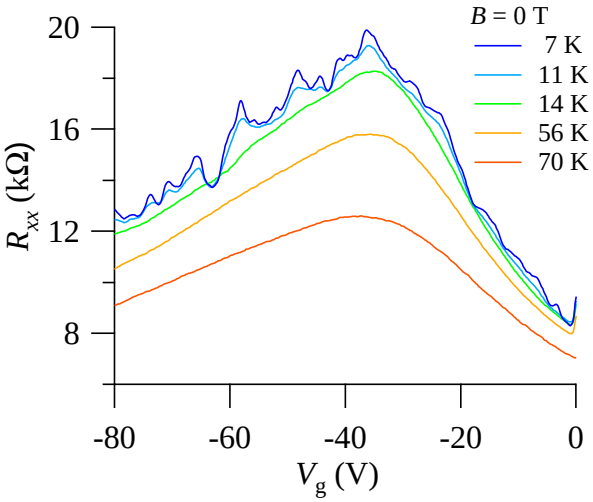

Figure 3. Observed resistance R_{xx} of a pristine graphene as a function of V_g for various temperatures.

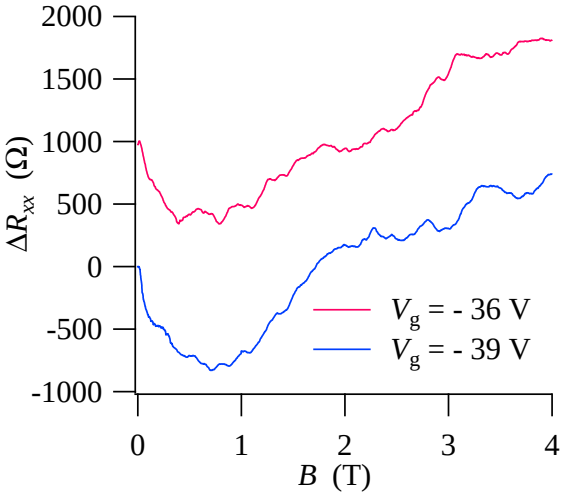

Figure 4. Magnetoresistance R_{xx} of a pristine graphene as a function of magnetic field B for two gate voltages V_g. The temperature is 7 K.

$T = 14$ K, the curve of R_{xx} is apparently smooth for the entire range of V_g. At $T = 11$ K, a subtle oscillation of the R_{xx} appears. As T decreases to 7 K, the amplitude of the oscillation grows more prominently. The pattern of the oscillation is fully reproducible, which is a typical manifestation of the universal conductance fluctuation (UCF) in the mesoscopic system. It should be also noted that the derivative of dR_{xx}/dT is negative everywhere in the whole range of V_g, which indicate that the graphene device is slightly insulative (not metallic), but here we emphasize that the monotonous dependence of R_{xx} on T is a key property.

To investigate the physical origin of such oscillations in detail, we measured the magnetoresistance R_{xx} for two different gate voltages at $V_g = -36\,\mathrm{V}$ and $V_g = -39\,\mathrm{V}$ at a low temperature of 7 K. In both cases, R_{xx} decreases as B increases in the weak magnetic field. As B increases more, R_{xx} turns to increase via the minima of R_{xx} that is located at $B_{\mathrm{min}} = 0.55\,\mathrm{T}$ at $V_g = -36\,\mathrm{V}$ and $B_{\mathrm{min}} = 0.70\,\mathrm{T}$ at $V_g = -39\,\mathrm{V}$. Here two gate voltages are chosen in the vicinity of the CNP, but these behaviors about B dependence of R_{xx} are similarly observed for the V_g far from the CNP.

The properties of R_{xx} in the low magnetic field limit are well explained by the weak localization (WL) theory in the bilayer graphene[4]. The interference of the electron waves that are scattered by disorders or impurities in the closed trajectories is weakened by the magnetic

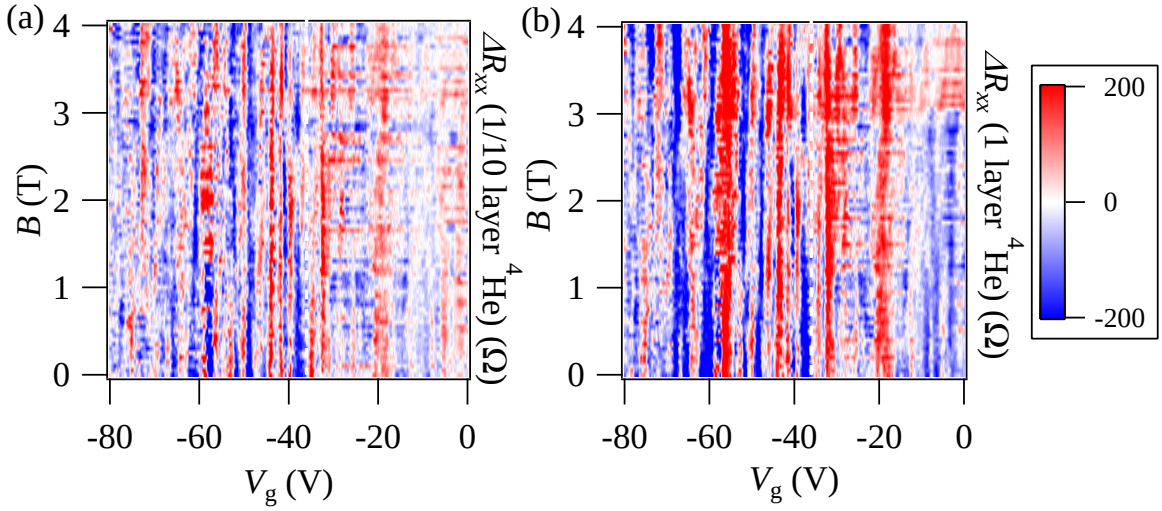

Figure 5. The magnetoresistance difference ΔR_{xx} between ^{4}He adsorbed graphene and pristine one as a function of B and V_g at $T = 7\,\mathrm{K}$. The adsorbed layer of ^{4}He is (a) 1/10 layers and (b) 1 layer.

field, resulting in a negative magnetoresistance. Since the interference of the electron waves in two different trajectories also causes the UCF of the order of e^2/h, where e is the elementary charge and h is the Plank constant, it concurs to the results of the magnetoresistance oscillation for both V_g and B in Fig. 3.

When $B > B_{\mathrm{min}}$, the conventional property of the observed enhancement in R_{xx} for increment of B implies that the crossover from WL to the strong Anderson localization. The R_{xx} behaviors are well analyzed by the model slightly modified from the equations for monolayer graphene suggested by McCann *et al.*[12] associated with various possible ways of breaking a 'hidden' valley symmetry of the graphene[13].

Figure 5 contains the most central part of this study. First, we pre-measure the magnetoresistance of the well-annealed pristine graphene $R_{xx}^{\mathrm{pristine}}$ as a function of B and V_g at $T = 7\,\mathrm{K}$. Afterward, we pour the ^{4}He gas to the sample cell through thin capillary from the room temperature, monitoring the decrement of the gas pressure in the constant volume. The adsorption energy of ^{4}He atom on graphite is about 12.2 K[14]. Though the binding energy of ^{4}He atom on graphene has not been experimentally observed yet, theory calculated it on the monolayer graphene about 13.4 K[15]. However, since we employ the bilayer graphene that is attached on the SiO_2 substrate, actual adsorption energy of ^{4}He on our sample may approach to the one on graphite. Thus we assume that adsorption energy of ^{4}He on graphene is nearly equivalent to the one on graphite, almost all ^{4}He atoms are homogenously adsorbed to mainly grafoil at $T = 7\,\mathrm{K}$, and we estimate the layer number of adsorbed ^{4}He atoms. We also measure the magnetoresistance with ^{4}He atoms, R_{xx}^{He}, as a function of B and V_g at $T = 7\,\mathrm{K}$. Then the difference $\Delta R_{xx} = R_{xx}^{\mathrm{He}} - R_{xx}^{\mathrm{pristine}}$ is demonstrated as an image plot for B and V_g in Fig. 5 for partial coverage of 1/10 (= 0.1) layers (a) and 1 layer (b) ^{4}He. The red and blue areas indicate the positive and negative change of magnetoresistance, respectively. The deeper colors represent the larger amplitude of ΔR_{xx}. The partial coverage of 1/10 layers is selected to attain the higher sensitivity on behalf of further investigation for 2D ^{4}He properties.

Firstly, at a glance of Fig. 5, overall colors of graph in Fig. 5(b) are darker than ones in Fig. 5(a). This fact suggests that the magnetoresistance is more influenced by the adsorption of larger amount of ^{4}He atoms. Secondly, the total amount of red areas and blue ones are

almost equal. The equality of the proportion of each area with different sign in ΔR_{xx} implies the changes of the resistance are NOT owing to the temperature variation, because the R_{xx} at 0 field monotonically depend on T. Finally, the shape of red and blue areas seems stripe extended to the vertical direction. It means that though ΔR_{xx} are strongly influenced by $V_{\rm g}$, it depends on B very weakly.

Here we discuss the effects of adsorbed inert atoms to electron transport in graphene and their mechanisms. As mentioned above, we could perfectly eliminate the possibility of sample heating by the thermal influx from the hot part of the cell to the sample. Therefore the R_{xx} change reflects intrinsic 2DEG properties. Now we focus on the relationship between the sign of ΔR_{xx} and the UCF oscillation. When we compare the ΔR_{xx} in Fig. 5 to $R_{xx}^{\rm pristine}$ carefully, we find the tendencies that the positive sign of ΔR_{xx} appears around the R_{xx} local maxima and negative one does around the R_{xx} local minima. These tendencies suggest that the ΔR_{xx} is significantly affected by the UCF pattern. The weak dependence of ΔR_{xx} on B at low magnetic field enlightens that the electron paths responsible for the interference does not change so much by the adsorption of ^{4}He atoms. However, the fact that 1 ^{4}He layer is more effectively change R_{xx} than 1/10 ^{4}He layers implies that the amplitude of the Coulomb potential that electrons feel caused by disorders or impurities of graphene varies by the adatoms, though the allocations of such defects, and thus electron paths, does not change drastically. Because the ^{4}He atoms are fully isotropic and Coulomb interactions between the ^{4}He atom and substrate are relatively small, the magnitude of ΔR_{xx} is also small. However, such subtle change of magnetoresistance may open the feasibility for detecting the intrinsic ^{4}He properties such as two dimensional Kosterlitz-Thouless type superfluid transition[16] or phase transition of two dimensional ^{4}He solid related to the commensurability[17]. Additionally, it should be noted that the phase diagram of ^{4}He on graphene is theoretically proposed[18], and thus the experimental investigation is invaluable. ΔR_{xx} is highly associated with the UCF, we infer that the more "dirty" graphene may be suitable for more sensitive detectors. Therefore the relationship between the density of the defects or impurities in artificially flawed graphene and the sensitivity as gas detectors should be further investigated.

In conclusion, we have carrid out the magnetotransport measurements of ^{4}He-adsorbed bilayer graphene at low temperature and the magnetic field B ranging from 0 to 4 T. The magnetoresistance difference ΔR_{xx} from the pristine graphene is observed as a function of gate voltage $V_{\rm g}$ and B for partial coverage of 1/10 (= 0.1) layers and one layer ^{4}He-adsorbed graphene. The overall magnitudes of ΔR_{xx} for one layer are larger than the one for 1/10 layer. Signs of ΔR_{xx} depend on the $V_{\rm g}$ for the entire range of B, associated with the magnetoresistance oscillation owing to the weak localization in the pristine graphene.

4. Acknowledgments

We acknowledge to A. Sawada and H. Yayama for the experimental setup at low temperature and high magnetic field with helium-free cryostat. We thank T. Nakajima for the machining the cryostat parts and the electronics of experiments. We are thankful to T. Terashima and S. Sasaki for utilizing the clean room facilities in the LTM center of Kyoto university. We are also thankful to A. Fujimoto for fruitful discussions about the weak localization of graphene. This research was performed under the Cooperative Research Program of "Network Joint Research Center for Materials and Devices". This work was supported by the "Topological Quantum Phenomena" (No. 25103722) Grant-in Aid for Scientific Research on Innovative Areas from the Ministry of Education, Culture, Sports, Science and Technology (MEXT) of Japan, JSPS KAKENHI Grant Number 24540331 and 25870966, Grants-in-Aid for Researchers from Hyogo College of Medicine (2010 for D. T. and 2011 for A. F.) and Grant for Basic Science Research Projects from the Sumitomo Foundation.

References

[1] Y. Zhang, Y. W. Tan, H. L. Stormer, and P. Kim, *Nature (London)* **438**, 201 (2005).
[2] K. S. Novoselov, A. K. Geim, S. V. Morozov, D. Jiang, M. I. Katsnelson, I. V. Grigorieva, S. V. Dubonos and A. A. Firsov, *Nature (London)* **438**, 197 (2005).
[3] K. S. Novoselov, E. McCann, S. V. Morozov, V. I. Fal'ko, M. I. Katsnelson, U. Zeitler, D. Jiang, F. Schedin and A. K. Geim, *Nat. Phys.* **2**, 177 (2006).
[4] R.V. Gorbachev, F.V. Tikhonenko, A. S. Mayorov, D.W. Horsell, and A. K. Savchenko, *Phys. Rev. Lett.* **98**, 176805 (2007)
[5] K. Kechedzhi, V. I. Fal'ko, E. McCann, and B. L. Altshuler, *Phys. Rev. Lett.* **98**, 176806 (2007)
[6] F. Schedin, A. K. Geim, S. V. Morozov, E. W. Hill, P. Blake, M. I. Katsnelson and K. S. Novoselov, *Nat. Mat.* **6**, 652 (2007).
[7] D. C. Elias, R. R. Nair, T. M. G. Mohiuddin, S. V. Morozov, P. Blake, M. P. Halsall, A. C. Ferrari, D. W. Boukhvalov, M. I. Katsnelson, A. K. Geim and K. S. Novoselov, *Science* **323**, 30 (2009). o, *Phys. Rev. Lett.* **98**, 176805 (2007)
[8] Y. Ohno, K. Maehashi, Y. Yamashiro, and K. Matsumoto, *Nano. Lett.* **9**, 3318 (2009).
[9] R. R. Nair, H. A. Wu, P. N. Jayaram, I. V. Grigorieva and A. K. Geim, *Science* **335**, 442 (2012).
[10] K. S. Novoselov, A. K. Geim, S. V. Morozov, D. Jiang, Y. Zhang, S. V. Dubonos, I. V. Grigorieva, A. A. Firsov, *Science* **306**, 666 (2004).
[11] A. C. Ferrari, J. C. Meyer, V. Scardaci, C. Casiraghi, M. Lazzeri, F. Mauri, S. Piscanec, D. Jiang, K. S. Novoselov, S. Roth, and A. K. Geim, *Phys. Rev. Lett.* **97**, 187401 (2006).
[12] E. McCann, K. Kechedzhi, V. I. Fal'ko, H. Suzuura, T. Ando, B. L. Altshuler, *Phys. Rev. Lett.* **97**, 146805 (2006).
[13] D. Terasawa, A Fukuda, Y. Ohno and K. Matsumoto, *to be published.*
[14] M. W. Cole and D. R. Frankl, *Rev. Mod. Phys.* **53**, 199 (1981).
[15] M. C. Gordillo and J. Boronat, *Phys. Rev. Lett.* **102**, 085303 (2009).
[16] D. J. Bishop and J. D. Reppy, *Phys. Rev. Lett.* **40**, 1727 (1978).
[17] D. S. Greywall and P. A. Busch, *Phys. Rev. Lett.* **67**, 3535 (1991).
[18] J. Happacher, P. Corboz, M. Boninsegni and L. Pollet, *Phys. Rev. B* **87**, 094514 (2013)